Organic & Biomolecular Chemistry

Accepted Manuscript

This article can be cited before page numbers have been issued, to do this please use: K. Khadka, S. Subedi, E. Oh and K. Lee, *Org. Biomol. Chem.*, 2025, DOI: 10.1039/D6OB00170J.

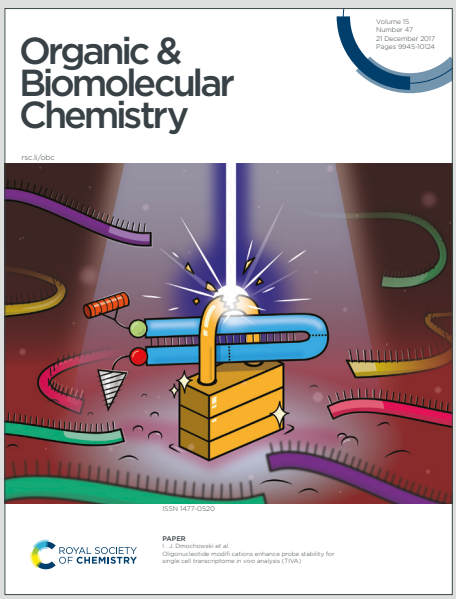

ROYAL SOCIETY OF CHEMISTRY

rsc.li/obc

View Article Online
DOI: 10.1039/D6OB00170J

Ultrafast Fluorescent Detection of Mercury(II) Ions in Aqueous and Biological Systems Using a Boronic Acid–Based Reaction Probe

Kishor Khadka[a], Sumita Subedi[a], Eun-Taex Oh[b], and Keun-Hyeung Lee[a,*]

[a]Education and Research Center for Smart Energy Materials and Process, Department of Chemistry and Chemical Engineering, Inha University, Incheon 402-751, South Korea

[b]Department in Biomedical Sciences, College of Medicine, Inha University, Incheon 22212, South Korea

E-mail: leekh@inha.ac.kr

View Article Online
DOI: 10.1039/D6OB00170J

Abstract

A new reaction-based fluorescent chemodosimeter for Hg^{2+} ions was developed based on the irreversible substitution reaction between Hg^{2+} and a phenylboronic acid moiety. The probe exhibits a rapid and highly selective fluorescence turn-on response toward Hg^{2+} with dual green and red emissions under visible-light excitation. Notably, the sensing reaction is completed within 2–3 min in aqueous solution at pH 7.4 containing only 1% organic solvent, demonstrating excellent reactivity under near-physiological conditions. The probe (**1**) forms a well-defined 1:1 covalent adduct with Hg^{2+}, avoiding complicated multi-adduct formation and enabling reliable quantitative detection. In addition, the boronic acid–based design effectively suppresses interference from competing metal ions. The probe shows efficient cellular uptake and allows real-time imaging of intracellular Hg^{2+} through simultaneous enhancement of green and red fluorescence signals. These results demonstrate that the present probe provides a robust sulfur-free platform for rapid, selective, and sensitive detection of mercury ions in aqueous environments and living cells, offering significant potential for environmental monitoring and biological mercury imaging.

Keywords: Hg^{2+}; Mercury(II); Boronic acid; Chemodosimeter; Turn-on fluorescence.

View Article Online
DOI: 10.1039/D6OB00170J

1. Introduction

Among mercury species, mercury ions (Hg^{2+}) pose a significant public health risk due to their persistence and high toxicity, because Hg^{2+} ions readily accumulate in the human body and can cause severe diseases.[1-3] Hg^{2+} ions are generated both naturally and as a result of increasing human activity,[1-3] leading to the contamination of aquatic environments and raising serious concerns about environmental and biological hazards. Because Hg^{2+} is bioavailable and can easily enter organisms via water, there is a critical need for methods capable of detecting Hg^{2+} sensitively and selectively in aqueous environments and live cells.

Among various analytical techniques, fluorescence-based sensors have emerged as powerful tools for mercury detection owing to their high sensitivity, operational simplicity, real-time response, and potential applicability to living systems.[4-14] In particular, reaction-based fluorescent probes (chemodosimeters) have been intensively investigated for the detection of Hg^{2+} ions in environmental and bio-samples because they offer high selectivity through irreversible chemical transformations induced by Hg^{2+}.[13-24] Unlike reversible coordination-based probes, chemodosimeters rely on irreversible chemical transformations, which provided significant fluorescent signal changes, generate accumulated fluorescence signals, and enable more reliable and unambiguous signal transduction.[5-8]

Among them, most Hg^{2+} chemodosimeters reported to date rely on the selective interaction between Hg^{2+} ions and sulfur-containing functional groups (Scheme 1a).[13-31] However, sulfur-based chemodosimeters often suffer from limited specificity and practical applicability due to cross-reactivity with other soft heavy metal ions, slow reactions in the presence of soft metal ions, and complicated reaction pathways. In addition, their sensing performance is frequently affected by oxidative conditions, which can suppress or distort the mercury-triggered desulfurization process, particularly in complex biological environments.

To overcome these intrinsic limitations, alternative sulfur-free reaction-based strategies have been actively explored.[5-8] Among them, boronic acid–based chemodosimeters have emerged as a promising platform for mercury sensing, as they rely on the irreversible substitution reaction of arylboronic acids with Hg^{2+} (Scheme 1b).[31-36] This reaction proceeds with high selectivity toward

View Article Online
DOI: 10.1039/D6OB00170J

Hg^{2+} and is largely unaffected by competing soft metal ions, thereby offering improved specificity, reproducibility, and reliability in aqueous and biological environments.

In our earlier studies, we introduced a fluorescent chemodosimeter based on the substitution reaction between Hg^{2+} ions and phenylboronic acid moieties. Although this approach successfully demonstrated the feasibility of sulfur-free mercury sensing, several intrinsic limitations remained. In aqueous media, the boronic acid–mercury reaction proceeded relatively slowly (>5 mins) or, in some cases, resulted in the formation of a 1:2 covalent adduct, which complicated signal interpretation and quantitative analysis.[31-36] In addition, boronic acid groups are known to strongly interact with diol-containing saccharides on cell surfaces, significantly impeding cellular uptake and thereby limiting the applicability of these probes for intracellular mercury detection.[33,34]

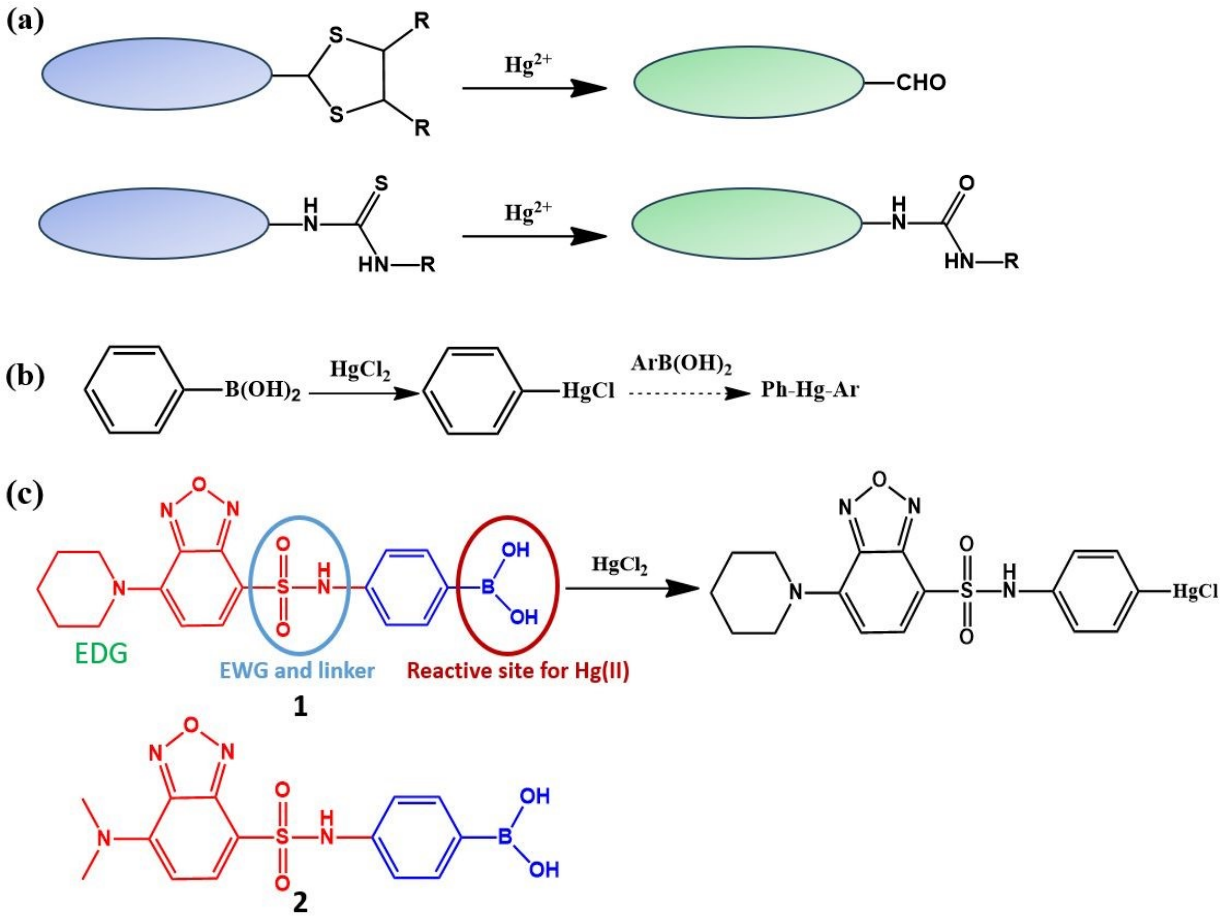

Scheme 1. (a) Some examples of chemical reaction for sulfur-based chemodosimeters for Hg^{2+}, (b) displacement reaction of a phenylboronic acid with Hg^{2+}, and (c) structure of a fluorescent chemodosimeters (**1** and **2**) containing a phenylboronic acid moiety.

View Article Online
DOI: 10.1039/D6OB00170J

In the present work, we report a new boronic acid–based fluorescent chemodosimeter (**1**) that overcomes these limitations (Scheme 1c). The probe is excitable with visible light and exhibits a pronounced turn-on fluorescence response, generating dual red and green emissions upon exposure to Hg^{2+} ions. Notably, the highly reactive probe displays an instantaneous fluorescence turn-on response (<2 min) in aqueous media containing only 1% organic solvent and forms a 1:1 covalent adduct with Hg^{2+}. Importantly, the probe readily penetrates living cells and enables intracellular Hg^{2+} detection, as evidenced by a significant enhancement of both red and green fluorescence signals. Collectively, these results represent a substantial advance in boronic acid–based mercury chemodosimeters and highlight their strong potential for real-time mercury sensing in complex biological and aqueous environments.

2. Experiments

2.1.Materials

4-Chloro-7-chlorosulfonyl-2,1,3-benzoxadiazole and 4-dimethylaminopyridine (DMAP) were purchased from TCI. 4-Aminophenylboronic acid pinacol ester, piperidine, and dimethylamine (in THF) were obtained from Sigma-Aldrich. Other reagents used for synthesis, including dichloromethane (DCM) and trifluoroacetic acid (TFA), were purchased from Acros Organics.

2.2. Synthesis of fluorescent probes

2.2.1. Synthesis of intermediate **3**

Probes were synthesized through the sulfonamide intermediate **3**, followed by nucleophilic substitution and subsequent boronate deprotection (Scheme S1).

4-Chloro-7-chlorosulfonyl-2,1,3-benzoxadiazole (253 mg, 1.0 mmol) and 4-aminophenylboronic acid pinacol ester (219 mg, 1.0 mmol) were dissolved in dry dichloromethane (20 mL). Triethylamine (279 μL, 2.0 mmol) was added dropwise, and the reaction mixture was stirred at 25 °C for 4 h. After removal of the solvent under reduced pressure, the crude product was purified

View Article Online
DOI: 10.1039/D6OB00170J

by silica gel column chromatography (particle size 0.063–0.200 mm) to afford the sulfonamide intermediate **3**.

*2.2.2. Synthesis of probe **1***

A solution of intermediate **3** (435 mg, 1.0 mmol) in dichloromethane was treated with piperidine (5 equiv., 494 μL) and 4-dimethylaminopyridine (DMAP, 12 mg, 0.1 equiv.). The reaction mixture was stirred at 40 °C for 6 h, and the reaction progress was monitored by thin-layer chromatography (TLC). After removal of the solvent under reduced pressure, the crude product was treated with a mixture of trifluoroacetic acid (TFA) and dichloromethane (DCM) (80:20, v/v, 20 mL) at room temperature for approximately 6 h to deprotect the pinacol boronate ester. The solvent was removed under reduced pressure, and the crude product was purified by silica gel column chromatography. The final product (**probe 1**) was further purified by preparative HPLC using a C18 column, and its purity was confirmed by analytical HPLC (Fig. S1).

*2.2.3. Synthesis of probe **2***

Probe **2** was prepared from intermediate **3** using the same procedure described above, except that dimethylamine (2 M in THF, 2.5 mL, 5 mmol) was used instead of piperidine in the nucleophilic substitution step. The crude product obtained after boronate deprotection was purified by silica gel column chromatography and further purified by preparative HPLC using a C_{18} column (Fig. S2).

The structures of probes **1**, **2**, and intermediate **3** were characterized by high-resolution mass spectrometry (HRMS) and ^{1}H and ^{13}C NMR spectroscopy (Figs. S3–S11).

Probe **1**; Orange solid; mp 118–120 °C; overall yield 54.6%.

^{1}H NMR (400 MHz, DMSO-d_6) δ 10.57 (s, 1H), 7.90 (d, J = 8.0 Hz, 1H), 7.52 (d, J = 8.4 Hz, 2H), 6.99 (d, J = 8.0 Hz, 2H), 6.46 (d, J = 8.4 Hz, 1H), 3.82 (s, 4H), 1.61 (s, 6H).

^{13}C NMR (101 MHz, DMSO-d_6) δ 146.4, 145.2, 142.9, 139.9, 139.8, 135.5, 117.7, 109.6, 104.0, 50.3, 25.7, 24.1.

HRMS (m/z): $[M + Na^+]^+$ calcd for $C_{17}H_{19}BN_4O_5SNa$, 425.10669; found 425.10645.

Probe **2:** Orange solid; mp 117 °C; overall yield 52.5%.

^{1}H NMR (400 MHz, DMSO-d_6) δ 10.51 (s, 1H), 7.90 (d, J = 8.8 Hz, 1H), 7.51 (d, J = 8.8 Hz, 2H), 6.97 (d, J = 8.8 Hz, 2H), 6.16 (d, J = 8.4 Hz, 1H), 3.40 (s, 6H).

View Article Online
DOI: 10.1039/D6OB00170J

^{13}C NMR (101 MHz, DMSO-d_6) δ 146.3, 145.2, 143.8, 140.0, 139.9, 135.5, 117.6, 107.8, 101.8, 42.9.

HRMS (m/z): $[M + Na^+]^+$ calcd for $C_{14}H_{18}BN_4O_5SNa$, 385.07539; found 385.07526.

Intermediate **3:** Yellow solid; mp 152–153 °C; yield 76.2%.

^{1}H NMR (400 MHz, DMSO-d_6) δ 11.07 (s, 1H), 8.10 (d, J = 8.8 Hz, 1H), 7.84 (d, J = 8.8 Hz, 1H), 7.59 (d, J = 8.8 Hz, 2H), 7.03 (d, J = 8.4 Hz, 2H).

^{13}C NMR (101 MHz, DMSO-d_6) δ 149.3, 145.3, 140.1, 136.6, 136.5,136.1, 131.2, 126.9, 126.8, 118.9, 114.7, 84.1, 83.4, 25.2, 25.1.

HRMS (m/z): $[M]^+$ calcd for $C_{18}H_{19}BClN_3O_5S$, 435.08270; found 435.0830.

2.3. UV- visible and fluorescence measurements

A stock solution of the probe (0.5 mM) was prepared in a mixed solvent of dimethylformamide (DMF) and distilled water (1:9, v/v). A stock solution of the probe was stable at 4 °C for at least four weeks, as verified by UV–visible absorption and fluorescence spectra. This stock solution was used for subsequent dilutions. A stock solution of $HgCl_2$ (0.5 mM) was prepared in distilled water. Fluorescence emission spectra were recorded in aqueous buffered solution (10 mM HEPES, pH 7.4) containing 1% DMF using a fluorescence spectrometer (Jasco FP-8500). The emission spectra were obtained with an excitation wavelength of 440 nm. UV–visible absorption spectra were recorded using a Jasco UV–visible spectrophotometer (V-750).

2.4. Determination of the limit of detection (LOD), quantum yield, and pK_a

The limit of detection (LOD) was determined by fluorescence titration experiments according to a reported method.[37] To evaluate the signal-to-noise (S/N) ratio, the fluorescence emission intensity of the blank sample was measured six times, and the standard deviation (σ) was calculated. The average fluorescence intensity was plotted as a function of analyte concentration to obtain the slope of the calibration curve (k). The LOD value was calculated using the equation LOD = 3σ/k.

The fluorescence quantum yields were determined using fluorescein as a reference standard (Φ = 0.79).

View Article Online
DOI: 10.1039/D6OB00170J

The pK_a value was measured based on the fluorescence intensity of probe **1** at different pH. The pK_a values were obtained by a nonlinear least square fitting of the data with the Henderson-Hasselbalch equation.

$$I = \frac{I_{max} \times 10^{(pH-pK_a)} + I_{min}}{1 + 10^{(pH-pK_a)}}$$

Where, I, I_{min} and I_{max}, are observed, minimum and maximum fluorescence intensity, respectively.

2.5. Fluorescent detection of Hg^{2+} in live cells by confocal microscopy

Cell viability assays and fluorescence imaging experiments were performed according to previously reported methods.[38] The fluorescence imaging procedure is briefly described as follows. A549 cells plated on chamber slides were incubated with probe 1 in DMEM medium containing 1% DMF at 37 °C for 8 h. After incubation, the probe-loaded cells were washed four times with phosphate-buffered saline (PBS) to remove excess probe. Subsequently, Hg^{2+} ions were added to the preloaded A549 cells and incubated for 30 min. Fluorescence images were then acquired using an inverted confocal laser scanning microscope (TE2000E, Nikon, Tokyo, Japan).

2.6. Quantification of Hg^{2+} ions in real-world samples

To evaluate the applicability of the probe for detecting Hg^{2+} ions in real water samples, tap water and groundwater samples were analyzed. The sample solutions were prepared by adding 10% (v/v) of tap water or groundwater to an aqueous buffered solution (10 mM HEPES, pH 7.4) containing 1% DMF. The fluorescence intensity at 585 nm was recorded in the presence of different concentrations of Hg^{2+} ions using standard solutions ranging from 0 to 1000 nM. The fluorescence intensities obtained from the sample solutions were then converted to Hg^{2+} concentrations using a calibration curve.

3. **Results and discussions**

*3.1. Design of fluorescent probe **1** based on phenylboronic acid as a reactive site for Hg^{2+}*

View Article Online
DOI: 10.1039/D6OB00170J

Most fluorescent probes for Hg^{2+} exhibit a turn-off response due to the strong fluorescence-quenching ability of Hg^{2+} ions.[5-8] However, turn-off–type detection suffers from critical limitations in practical applications, as fluorescence decreases can also arise from probe precipitation, nonspecific environmental quenching, or absorption by unknown impurities, leading to ambiguous signal interpretation. To overcome these drawbacks, we designed turn-on fluorescent probes in which an intramolecular charge transfer (ICT) fluorophore, benzofurazan moiety, is conjugated to a phenylboronic acid moiety through a thioamide linker (Scheme 1c). In this design, the phenylboronic acid functions as the reactive site for Hg^{2+}, while the benzofuranzan moiety was used as a fluorophore.[39] The thioamide group serves as a linker between the fluorophore and the reactive site and an electron withdrawing group. Piperidine was introduced as the electron-donating group of the ICT fluorophore part of probe **1**, whereas dimethylamine was conjugated as the electron-donating group of the ICT fluorophore part of probe **2** because piperidine provides improved quantum yield and photostability compared to commonly used dimethylamine donors.[40] Both fluorescent probes were designed to be excitable with visible light and to exhibit a broad, long-wavelength emission profile, including green and red emissions. These optical features effectively minimize background interference from complex biological environments and are advantageous for biological and environmental mercury sensing.

*3.2. Synthesis and photophysical properties of fluorescent probe **1** and **2***

Probes **1** and **2** were synthesized through a two-step sequence via the sulfonamide intermediate **3** (Scheme S1). The sulfonyl chloride group of 4-chloro-7-chlorosulfonyl-2,1,3-benzoxadiazole was first coupled with 4-aminophenylboronic acid pinacol ester in the presence of triethylamine to afford intermediate **3**. Subsequent nucleophilic substitution of the chloro group with piperidine or dimethylamine provided the corresponding intermediates, which were finally converted to probe **1** and probe **2**, respectively, through deprotection of the pinacol boronate ester using TFA/DCM. The successful synthesis and high purity of the probes were confirmed by ^{1}H NMR, ^{13}C NMR, mass spectrometry, and HPLC analyses.

According to our design concept, both fluorescent probes are excited with visible light and showed green and red emission ranging from 550 nm to 650 nm in purely aqueous solutions. As the poor water solubility of many fluorescent probes limits their practical applications in biological

View Article Online
DOI: 10.1039/D6OB00170J

and aqueous environments, we evaluated the solubility of probes **1** and **2** in aqueous solution (pH 7.4) containing 1% DMF. Both probes exhibited good solubility under these conditions, as evidenced by a linear correlation between absorbance and concentration over the range of 0–25 μM (Fig. 1a–c). Upon excitation at 440 nm, probes **1** and **2** displayed broad emission bands spanning 530–730 nm, and the fluorescence intensity increased linearly with concentration over the same range (0–25 μM). In addition, the relative fluorescence intensities of both probes were monitored for 180 min under continuous visible-light irradiation, demonstrating sufficient photostability in aqueous solution containing 1% DMF.

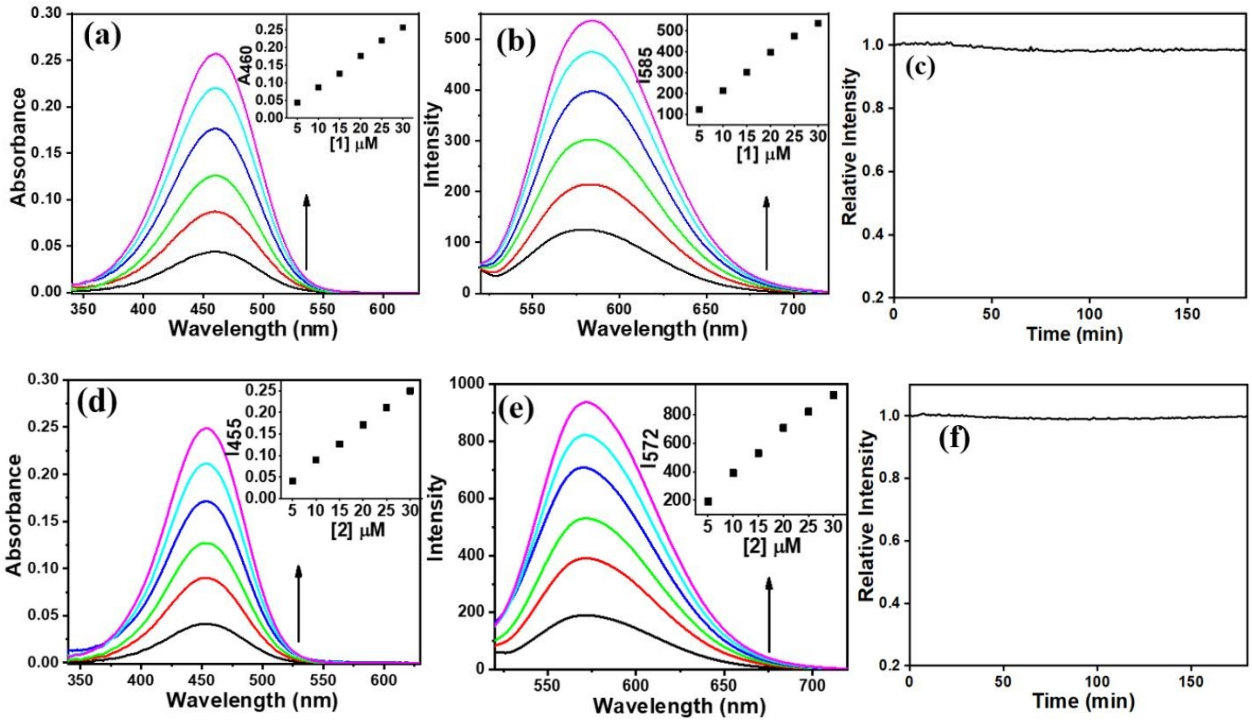

Figure 1. (a. d) UV–visible absorption spectra and (b, e) fluorescence emission spectra of probe (**1** and **2**) at different concentrations (λ_{ex} = 440 nm) and (c, f) time-dependent relative fluorescence intensity changes of **1** and **2** over 150 min in aqueous buffered solution (10 mM HEPES, pH 7.4) containing 1% DMF.

3.3. Fluorescent responses of chemodosimeters to Hg^{2+} and characterization of the reaction product

View Article Online
DOI: 10.1039/D6OB00170J

Fluorescence titration experiments of the fluorescent chemodosimeters with Hg^{2+} were conducted in aqueous solution (10 mM HEPES, pH 7.4) containing 1% DMF (Fig. 2a,e). Upon gradual addition of Hg^{2+}, pronounced fluorescence enhancement was observed for both probes over the emission range of 450–650 nm. Specifically, the emission intensity at 585 nm increased by approximately fourfold for probe **1**, whereas a twofold increase was observed for probe **2**.

Notably, probe **1** exhibited mainly fluorescence intensity enhancement with little change in the emission wavelength, whereas probe **2** showed a slight red shift in the emission spectrum upon reaction with Hg^{2+}. This difference can be attributed to the stronger electron-donating ability of the piperidine group in probe **1** compared with the dimethylamine group in probe **2**, which results in a stronger ICT character and thus minimizes spectral shifts while enhancing fluorescence intensity. In contrast, the weaker donor in probe **2** leads to a slightly greater redistribution of the ICT state upon formation of the arylmercury(II) chloride species, giving rise to the observed bathochromic shift.

Interestingly, both probes exhibited exceptionally rapid responses toward Hg^{2+} (Fig. 2b and 2f). The fluorescence enhancement reached completion within 2–3 min after Hg^{2+} addition, and even at a low Hg^{2+} concentration (1 μM), the fluorescence response was completed within 120 s. These results demonstrate the high reactivity and rapid sensing capability of the probes toward Hg^{2+} in aqueous media.

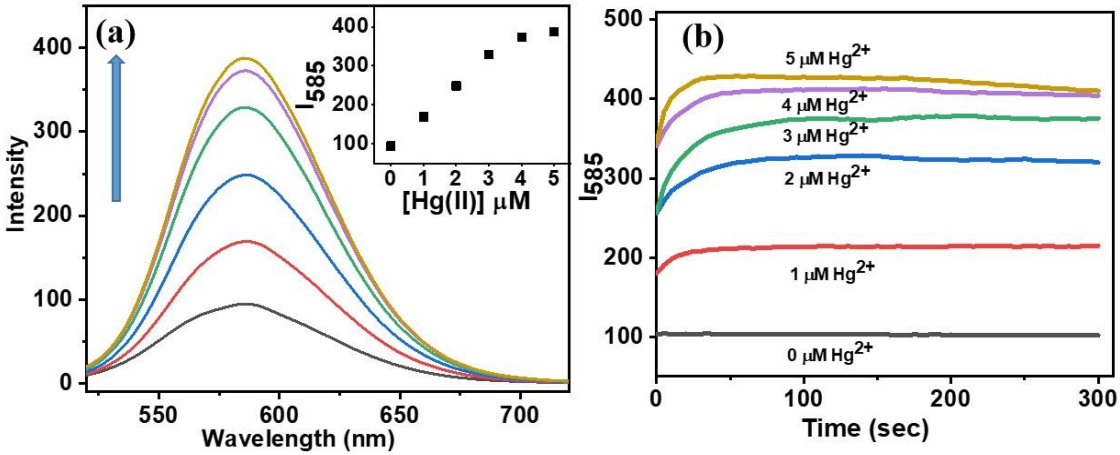

View Article Online
DOI: 10.1039/D6OB00170J

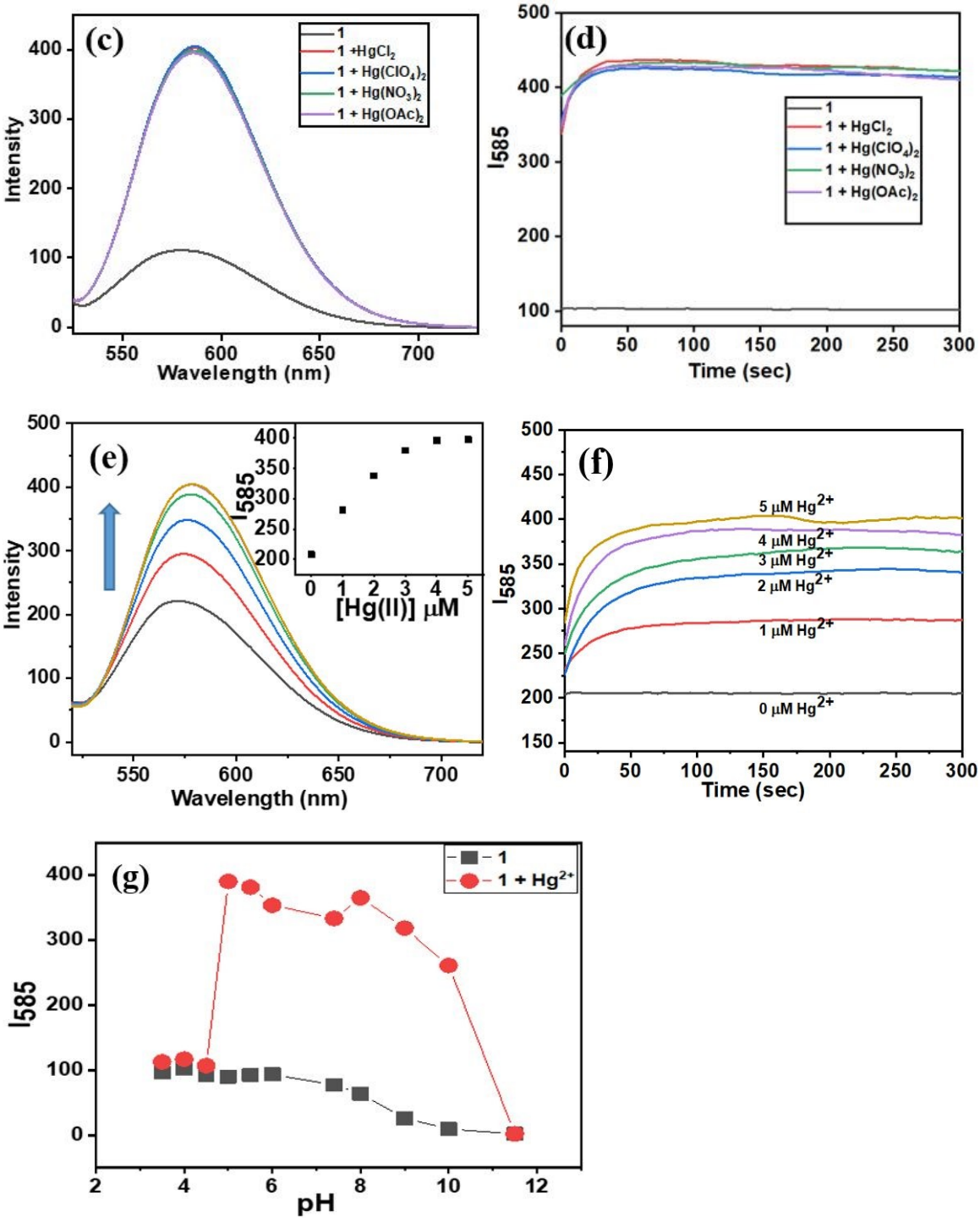

Figure 2. (a) Fluorescence emission spectra and (b) time-dependent emission intensity at 585 nm of probe **1** (5 μM) in the presence of Hg^{2+} (0–5 μM). (c and d) Fluorescence emission spectra and time-dependent emission intensity of probe **1** with various mercury salts (5 μM) after 2 min incubation in aqueous buffered solution (pH 7.4) containing 1% DMF. (e) Fluorescence emission spectra and (f) time-dependent emission intensity at 585 nm of probe **2** (5 μM) in the presence of

View Article Online
DOI: 10.1039/D6OB00170J

Hg^{2+} (0–5 μM). (g) Emission intensity changes of probe **1** in the presence of Hg^{2+} at different pH values.

To evaluate the influence of counter anions, the fluorescence responses of the probes to different mercury salts, including $HgCl_2$, $Hg(ClO_4)_2$, $Hg(NO_3)_2$, and $Hg(OAc)_2$, were examined (Fig. 2c, 2d and Fig. S12). All mercury salts produced nearly identical final fluorescence intensities within 3 mins, regardless of the anionic species. This observation confirms that the reaction-based sensing process of the probes toward Hg^{2+} proceeds efficiently and is essentially independent of the counter anion, indicating negligible anion effects on both detection sensitivity and response kinetics.

As probe **1** exhibited a more pronounced fluorescence enhancement in response to Hg^{2+} than probe **2**, we further investigated the effect of pH on the Hg^{2+} sensing performance of probe **1** (Fig. 2g). As the pH increased above 8.0, the fluorescence enhancement induced by Hg^{2+} gradually decreased, which can be attributed to the formation of insoluble mercury species such as $Hg(OH)_2$, leading to reduced availability of free Hg^{2+} ions. When the pH decreased from 8.0 to 5.0, the fluorescence enhancement remained significant. However, a pronounced decrease in emission intensity was observed at pH 4.5, which is attributed to the protonation of the cyclohexylamine group in the fluorophore moiety of the probe ($pK_a \approx 4.5$),[12,41] resulting in disruption of the intramolecular charge transfer process. These results indicate that the probe exhibits optimal sensing performance toward Hg^{2+} over a wide pH range (5–9), including physiological pH, demonstrating its suitability for both biological and environmental applications.

To verify the irreversible nature of the reaction between **1** and Hg^{2+}, EDTA, a strong reversible chelator for Hg^{2+}, was employed (Fig. 3a). After completion of the fluorescence enhancement induced by Hg^{2+}, subsequent addition of EDTA caused no noticeable change in the fluorescence spectrum. This result indicates that Hg^{2+} was irreversibly consumed during the sensing reaction.

In addition, EDTA was added simultaneously with Hg^{2+} to examine whether EDTA interferes with the sensing process of **1**. Under these conditions, the fluorescence intensity change of the reaction-based probe was almost identical to that observed in the absence of EDTA, demonstrating that EDTA does not inhibit the Hg^{2+}-triggered irreversible reaction. Overall results confirm that probe

View Article Online
DOI: 10.1039/D6OB00170J

1 detects Hg^{2+} through an irreversible reaction mechanism, and that this reaction is not affected by the presence of EDTA.

The reaction product of **1** with Hg^{2+} was further analyzed by C_{18}-TLC, HPLC, and mass spectrometry (Fig. 3b, 3c, and Fig. S13). Probe **1** was incubated with Hg^{2+} in distilled water containing 20% CH_3CN for 5 min, and the resulting major product was analyzed by HPLC–ESI mass spectrometry. A new spot/peak with lower polarity (higher hydrophobicity) than that of probe **1** was observed in both the TLC and HPLC chromatograms. ESI mass spectrometric analysis revealed a molecular ion peak at *m/z* 559.3, corresponding to an arylmercury species (Scheme 1), supporting the replacement reaction of the phenylboronic acid moiety with Hg^{2+}. Further analysis of the product by FAB mass spectrometry confirmed this transformation, resulting in the formation of an arylmercury(II) chloride (ArHgCl) species (Fig. S14).

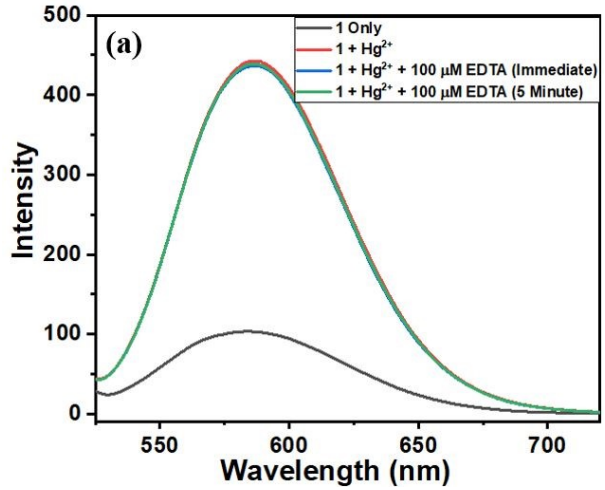

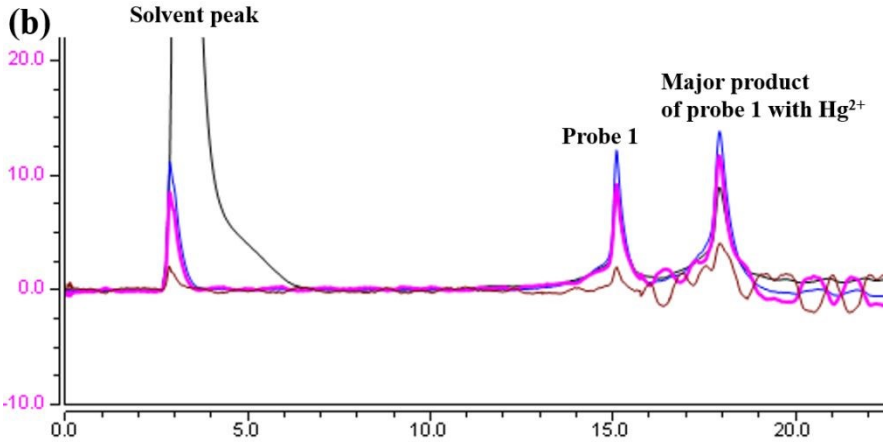

View Article Online
DOI: 10.1039/D6OB00170J

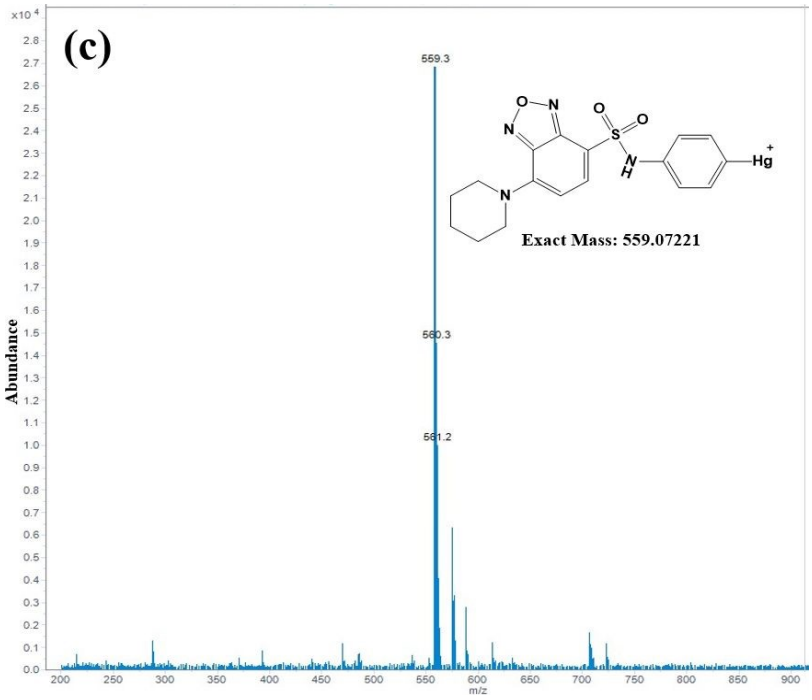

Figure 3. (a) Fluorescence emission spectra of probe **1** (5 μM) with Hg^{2+} (5 μM) in the presence of EDTA (100 μM) in aqueous buffered solution (10 mM HEPES, pH 7.4) containing 1% DMF, and (b) HPLC analysis, and (c) mass spectrometric analysis of the reaction product using ESI mass spectrometry.

3.4. Selectivity study of fluorescent chemodosimeter (1)

The selectivity of probe **1** toward Hg^{2+} was evaluated by measuring its fluorescence response to various metal ions, including Na^{+}, Mg^{2+}, Ca^{2+}, Al^{3+}, Cr^{3+}, Co^{2+}, Ni^{2+}, Mn^{2+}, Cu^{2+}, Zn^{2+}, Cd^{2+}, Ag^{+}, Pb^{2+}, K^{+}, and Hg^{2+}, in aqueous buffered solution (10 mM HEPES, pH 7.4) containing 1% DMF (Fig. 4a). Among all tested metal ions, only Hg^{2+} induced a significant fluorescence enhancement, while the other metal ions produced negligible changes. This result confirms that the phenylboronic acid–based displacement reaction is highly selective for Hg^{2+} in aqueous solutions.

Encouraged by these results, we next investigated the fluorescence response of probe **1** to Hg^{2+} in the presence of competing metal ions (Fig. S15). Even in the presence of Group I and Group II metal ions (1 mM) and other heavy metal ions (10 μM), the fluorescence enhancement induced by Hg^{2+} was not significantly affected. However, a noticeable decrease in the Hg^{2+}-induced fluorescence enhancement was observed in the presence of coexisting Cu^{2+} ions. The suppressed fluorescence response toward Hg^{2+} in the presence of Cu^{2+} is not attributed to a direct fluorescence

View Article Online
DOI: 10.1039/D6OB00170J

quenching effect, because the addition of Cu^{2+} after completion of the Hg^{2+}-triggered reaction did not affect the emission intensity. Instead, Cu^{2+} is likely to interfere with the Hg^{2+}-induced reaction by forming a coordination complex with the boronic acid moiety, thereby reducing the reactivity of the probe toward Hg^{2+}. Thus, the inhibitory effect of Cu^{2+} on the Hg^{2+}-induced fluorescence response was completely removed by EDTA. In the presence of EDTA, the probe exhibited the same fluorescence enhancement upon simultaneous addition of Hg^{2+} and Cu^{2+} as that observed with Hg^{2+} alone (Fig. 4b), confirming that Cu^{2+} interferes with the sensing process through reversible coordination rather than fluorescence quenching. These results demonstrate that EDTA effectively masks Cu^{2+}, thereby preventing its inhibitory interaction with the boronic acid moiety and restoring the intrinsic Hg^{2+}-triggered fluorescence response.

This observation indicates that probe **1** can selectively detect Hg^{2+} without significant interference from coexisting metal ions. The selectivity was further visualized by naked-eye observation under UV illumination (Fig. 4c). Only the Hg^{2+}-treated solution exhibited a distinct red emission, whereas no noticeable fluorescence color change was observed in the presence of other metal ions. These results clearly demonstrate the excellent visual selectivity of probe **1** for Hg^{2+}.

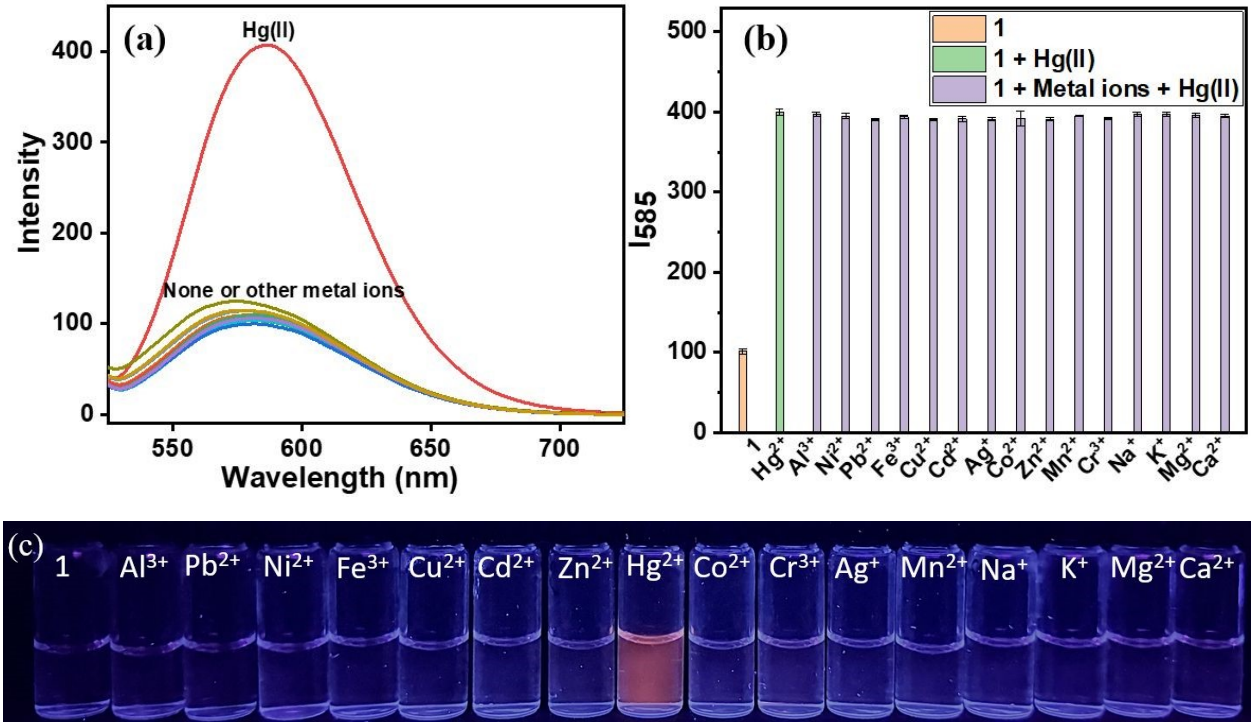

View Article Online
DOI: 10.1039/D6OB00170J

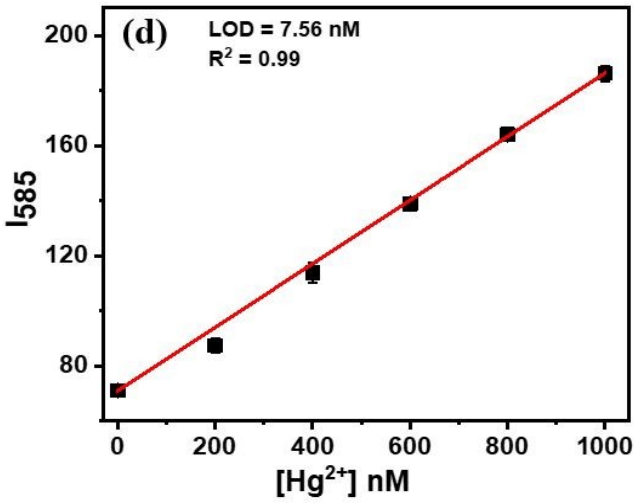

Figure 4. (a) Fluorescence emission spectra of probe **1** with various metal ions, (b) fluorescence emission intensity of **1** with Hg^{2+} in the presence of coexisting metal ions, (c) fluorescence photographs of **1** with various metal ions under UV irradiation, and (d) linear emission intensity change of **1** with Hg^{2+} in aqueous buffered solution (10 mM HEPES, pH 7.4) containing 1% DMF. The concentrations of probe **1**, heavy metal ions, and Group I and II metal ions were 5 μM, 10 μM, and 1000 μM, respectively.

The detection limit of probe **1** for Hg^{2+} was determined based on the fluorescence intensity at 585 nm (Fig. 4d). The limit of detection was calculated to be 7.56 nM ($R^2 = 0.99$) in aqueous buffered solution (10 mM HEPES, pH 7.4). This detection limit is comparable to the maximum allowable concentration of mercury ions in drinking water (10 nM, 2 ppb) established by the U.S. Environmental Protection Agency (EPA).

The low limit of detection (LOD) and the negligible interference from other metal ions demonstrated the practical applicability of probe **1** for environmental mercury monitoring. To further evaluate its practical utility, probe **1** was applied to quantify Hg^{2+} in real water samples, including groundwater (GW) and tap water (TW). To validate the analytical performance, known amounts of Hg^{2+} were spiked into GW and TW samples, and the concentrations were determined using the fluorescence emission intensity of probe **1** (Table S1). The recovery values for Hg(II) ranged from 92.9% to 99.9% in GW and from 94.3% to 101.1% in TW. These satisfactory recovery results indicate that probe 1 can be reliably applied for the quantitative determination of Hg^{2+} in real aqueous samples.

View Article Online
DOI: 10.1039/D6OB00170J

The fluorescent probe based on the reaction of phenylboronic acid with Hg^{2+} exhibited higher selectivity for Hg^{2+} than most previously reported fluorescent chemodosimeters that rely on sulfur-based reactions with Hg^{2+}. Considering the detection characteristics of the reported fluorescent chemodosimeters (Table S2), probe **1** displayed several notable sensing properties, including visible-light excitation, enhancement of red fluorescence upon exposure to Hg^{2+}, operation in a purely aqueous solution containing only 1% organic solvent, and a fast response to low concentrations of Hg^{2+}.

*3.5. Fluorescence imaging of Hg^{2+} in live cells Using chemodosimeter **1***

Since probe **1** exhibited a sensitive turn-on fluorescence response to Hg^{2+} in aqueous buffered solution at pH 7.4, we further investigated its applicability for Hg^{2+} detection in live human cells.

The cytotoxicity of **1** toward A549 cells was evaluated using an ATP-Glo assay. As shown in Fig. S16, incubation with **1** at concentrations ranging from 0 to 30 μM for 24 h did not cause any significant reduction in cell viability, indicating good biocompatibility of the probe within this concentration range.

For fluorescence imaging experiments, A549 cells were incubated with probe **1** (10 μM) at 37 °C for 8 h, followed by treatment with various concentrations of Hg^{2+}. As shown in Fig. 5a, cells treated with **1** alone exhibited only weak background fluorescence in both the green and red channels. In contrast, upon addition of Hg^{2+}, a gradual and concentration-dependent enhancement of both green and red fluorescence emissions was clearly observed. Consequently, the merged fluorescence images displayed an increasing yellow signal with increasing Hg^{2+} concentration. These results demonstrate that probe **1** efficiently penetrates cell membranes and sensitively detects intracellular Hg^{2+} through a fluorescence turn-on response.

View Article Online
DOI: 10.1039/D6OB00170J

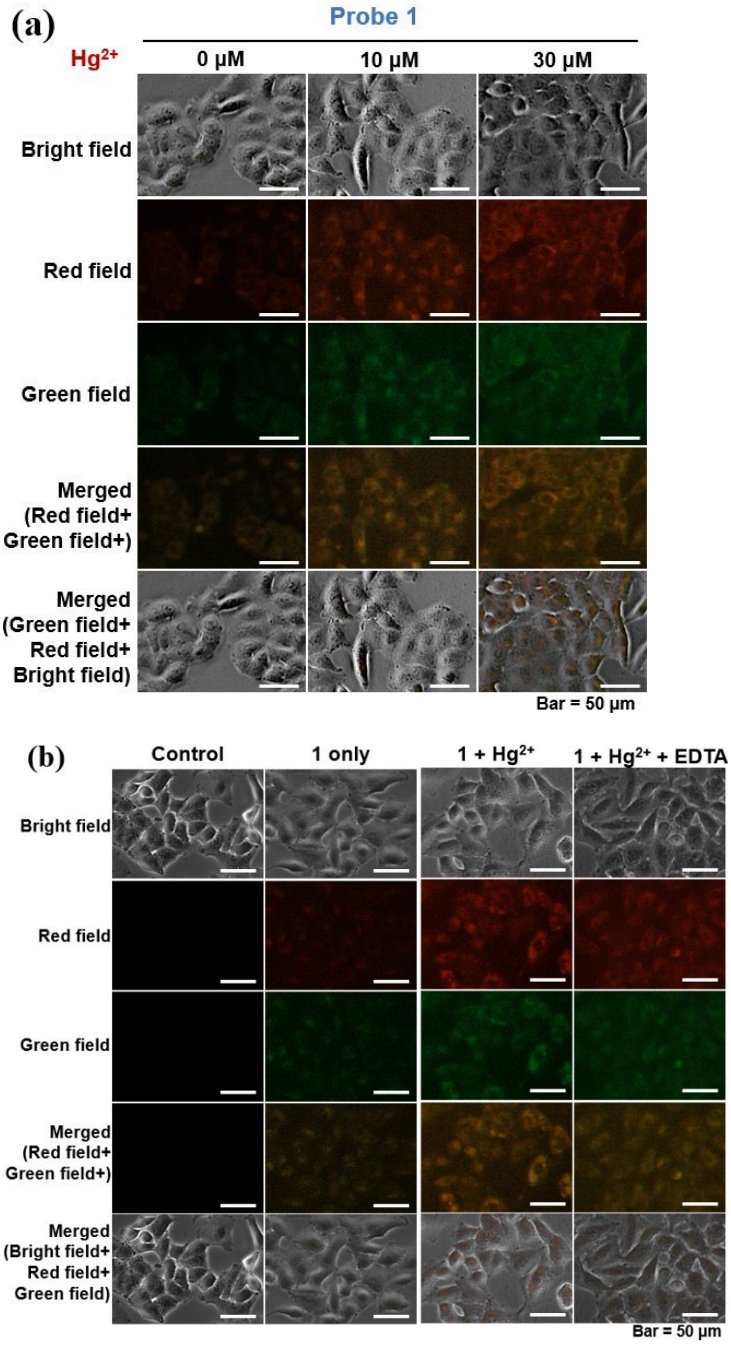

Figure 5. (a) Confocal fluorescence images of cells incubated with probe **1** (10 μM) in the presence of Hg^{2+} at concentrations of 0, 10, and 30 μM. (b) Confocal fluorescence images of cells treated with probe **1** (10 μM) and Hg^{2+} (10 μM) followed by subsequent addition of EDTA (300 μM).

View Article Online
DOI: 10.1039/D6OB00170J

To further examine the irreversibility of the fluorescence response, cell-permeable EDTA was added to the cells containing probe **1** and Hg^{2+}, which exhibited strong red and green emissions. As shown in Fig. 5b, the addition of EDTA did not induce a significant decrease in either green or red fluorescence intensities. This observation confirms that the fluorescence enhancement does not arise from reversible Hg^{2+} coordination, but rather from an irreversible chemical reaction between chemodosimeter **1** and Hg^{2+}. These results clearly demonstrate that chemodosimeter **1** enables highly sensitive turn-on fluorescence detection of Hg^{2+} in living cells. More importantly, the irreversible reaction between **1** and Hg^{2+} proceeds efficiently even within the highly complex intracellular environment.

*3.6. Binding mode and self-activation mechanism of chemodosimeter **1** toward Hg^{2+}*

UV–vis absorption titration experiments were performed to investigate the binding mode between probe 1 and Hg^{2+}. Upon gradual addition of Hg^{2+}, the absorption band of 1 centered at 460 nm exhibited a distinct red shift (Fig. 6a). This spectral change can be attributed to the formation of a covalent aryl–Hg^{+} adduct (Fig. 3c), in which the Hg^{+} moiety acts as a stronger electron-withdrawing group than the original boronic acid functionality. This substitution enhances the intramolecular charge transfer character of the fluorophore part, leading to a bathochromic shift and increased fluorescence emission. Consistently, the fluorescence quantum yield ($\phi = 0.022$) of the reaction product measured in aqueous solution was significantly higher than that of the parent probe ($\phi = 0.0083$), confirming that replacement of the boronic acid group by Hg^{2+} substantially improves the fluorescence efficiency.

To understand the origin of the ultrafast response of **1** toward Hg^{2+}, we considered the reaction mechanism between phenylboronic acid and Hg^{2+}.[42,43] This transformation is generally described as an electrophilic substitution–assisted transmetalation process (Fig. 6b), in which the boronate form is more reactive than the neutral boronic acid species. Accordingly, the pK_a value of the phenylboronic acid moiety in probe **1** was determined (Fig. S17). The obtained pK_a value of 8.3 indicates that the neutral boronic acid form predominates at physiological pH (7.4), which alone cannot explain the exceptionally fast reaction rate.

View Article Online
DOI: 10.1039/D6OB00170J

We therefore propose that the ultrafast response arises from an intermolecular self-activation mechanism mediated by supramolecular dimer formation (Fig. 6b). In aqueous media containing a low fraction of organic solvent, the amphiphilic nature of probe **1** promotes the formation of supramolecular dimeric assemblies. In these assemblies, the aromatic moieties stack through hydrophobic interactions, while the thioamide groups further stabilize the structure via intermolecular hydrogen bonding. Within this dimeric arrangement, the piperidine unit of one molecule is positioned in close proximity to the boronic acid group of the neighboring molecule. This spatial organization enables an intermolecular acid–base interaction, in which the basic piperidine nitrogen partially deprotonates the boronic acid moiety ($pK_a \approx 8.3$), generating a boronate-like activated species even under physiological pH conditions. Consequently, intermolecular acid–base interaction may enhance the aromatic substitution reaction with Hg^{2+}, leading to a dramatically accelerated reaction rate.

Three experimental observations strongly support this self-activation model. First, dimeric species were directly observed in the ESI mass spectrum (Fig. 6c). Although the ionization process generally induces dissociation of noncovalent aggregates due to charge repulsion, a distinct peak at *m/z* 805.4 was detected, which corresponds to the protonated dimeric species ($2 \times 403.2 + H^+$). The persistence of this dimeric ion under high-energy ionization conditions strongly indicates that probe **1** has an intrinsic propensity to form dimeric assemblies in solution, thereby supporting the feasibility of dimer formation in aqueous environments.

Second, organic solvent was introduced to disrupt the dimeric assembly of **1** and to examine its effect on the reaction kinetics with Hg^{2+} (Fig. 6d). As the DMF content increased from 1% to 20%, the fluorescence response became markedly slower. This pronounced retardation of the reaction clearly indicates that the dimeric assemblies in aqueous media play a critical role in facilitating the self-activation process toward Hg^{2+}. The reaction kinetics of the probe were investigated under different solvent conditions. In the presence of 10% and 20% DMF, the reaction rate between the probe and Hg^{2+} could be reliably monitored (Fig. S18). To determine the reaction order with respect to the probe, the concentration of Hg^{2+} was fixed at ten times that of the probe to maintain pseudo-first-order conditions. The reaction rates were measured at various probe concentrations, and a plot of ln(rate) versus ln[probe] was used to determine the reaction order (Fig. 6e and 6f).

View Article Online
DOI: 10.1039/D6OB00170J

Under 20% DMF conditions, the reaction order with respect to the probe concentration was determined to be 0.92, indicating an approximately first-order dependence. In contrast, under 10% DMF conditions, the reaction order increased to 1.76. This higher reaction order strongly suggests the involvement of probe dimerization and supports the proposed dimeric self-activation mechanism of the fluorescent probe. In 1% DMF, the reaction proceeded too rapidly to accurately determine the reaction order with respect to the probe concentration. Overall, this dimeric self-activation mechanism effectively converts the boronic acid moiety into a highly reactive boronate-like species without requiring alkaline conditions.

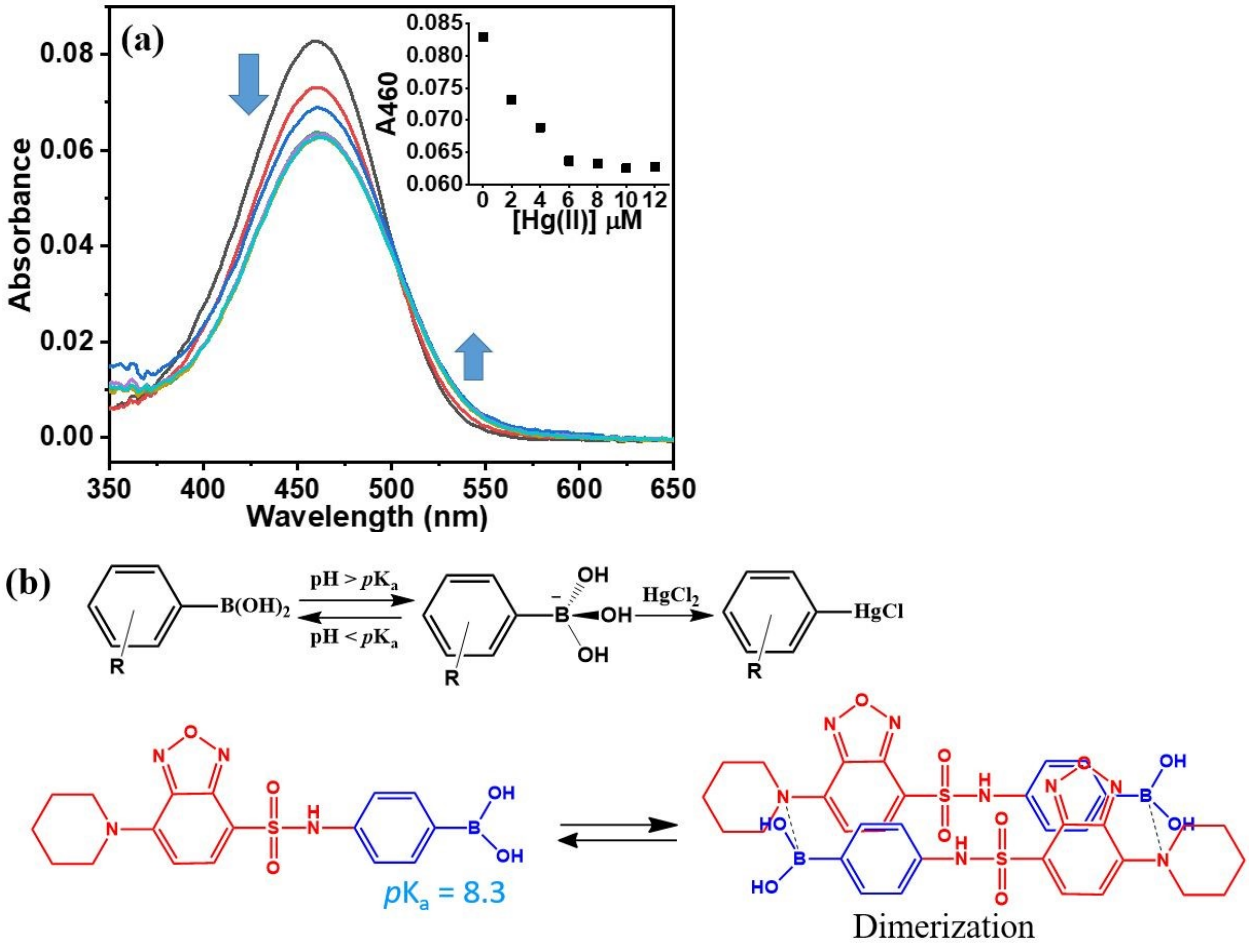

View Article Online
DOI: 10.1039/D6OB00170J

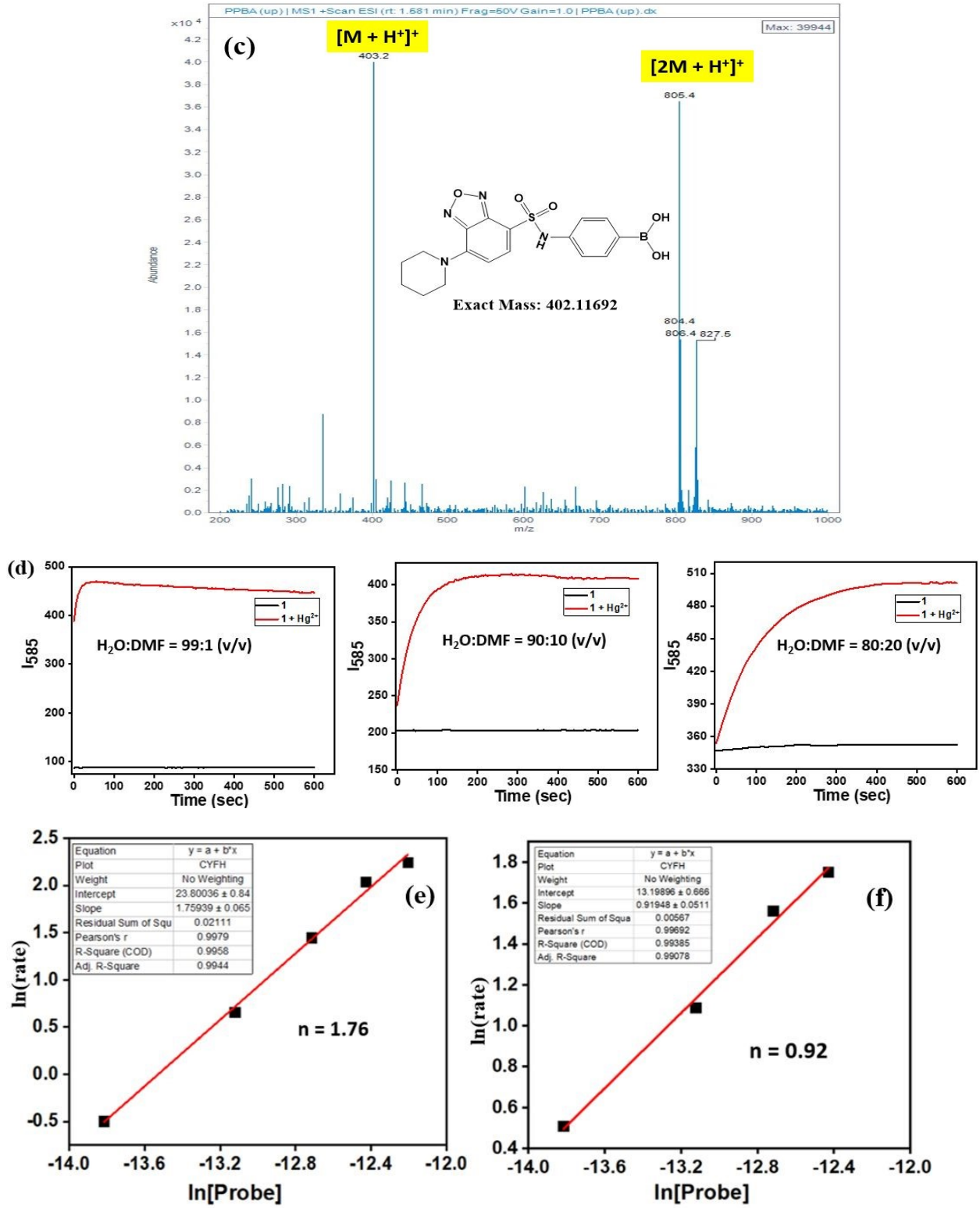

Figure 6. (a) UV–visible absorption titration spectra of probe **1** (10 μM) in the presence of Hg^{2+}. (b) Proposed reaction mechanism of the phenylboronate moiety with Hg^{2+} and the intermolecular self-activation mechanism of probe **1** for reaction with Hg^{2+}. (c) ESI mass spectrometric analysis

View Article Online
DOI: 10.1039/D6OB00170J

of the dimeric form of **1** in aqueous solutions. (d) Time-dependent fluorescence intensity profiles of **1** (10 μM) with Hg^{2+} (10 μM) as a function of DMF content (%). Linear analysis of ln(reaction rate) vs ln[probe] in aqueous solution (10 mM HEPES, pH 7.4) including (e) 10% DMF and (f) 20% DMF.

4. Conclusions

In summary, we developed a new boronic acid–based reaction-type fluorescent chemodosimeter for the selective and rapid detection of Hg^{2+} ions. The probe (**1**) operates through an irreversible substitution reaction between the phenylboronic acid moiety and Hg^{2+}, producing a stable 1:1 covalent adduct accompanied by a pronounced dual-channel fluorescence turn-on response. The present probe exhibits excellent selectivity, minimal interference from competing metal ions, and a remarkably fast response time within 2–3 min in nearly pure aqueous solutions. Furthermore, the probe readily penetrates living cells and enables real-time visualization of intracellular Hg^{2+} through both green and red fluorescence channels.

These features collectively overcome key limitations of previous boronic acid–based mercury probes, including slow reaction kinetics, poor aqueous reactivity, and limited cellular uptake. Therefore, this work provides a significant advancement in sulfur-free mercury chemodosimeter design and offers a promising molecular platform for practical mercury detection in complex environmental and biological systems.

Conflicts of interest

There are no conflicts to declare.

Acknowledgments

This work was supported by grant from Inha University.

Appendix A. Supplementary data

All data supporting this study are included in the Electronic Supplementary Information (ESI).

Supplementary data to this article can be found online at

View Article Online
DOI: 10.1039/D6OB00170J

Notes and references

1 U.S. Environmental Protection Agency, *Mercury Update: Impact on Fish Advisories*, EPA Fact Sheet EPA-823-F-01-011, Office of Water, Washington, DC, 2001.

2 W. F. Fitzgerald, C. H. Lamborg and C. R. Hammerschmidt, *Chem. Rev.*, **2007**, *107*, 641–662.

3 Y.-S. Hong, Y.-M. Kim and K.-E. Lee, *J. Prev. Med. Public Health*, **2012**, *45*, 353–363.

4 B. Valeur and M. N. Berberan-Santos, *Molecular Fluorescence: Principles and Applications*, 2nd edn, Wiley-VCH, Weinheim, 2012, pp. 479–531.

5 H. Shuai, C. Xiang, L. Qian, F. Bin, L. Xiaohui, D. Jipeng, Z. Chang, L. Jiahui and Z. Wenbin, *Dyes Pigm.*, **2021**, *187*, 109125.

6 M. Saleem, M. Rafiq and M. Hanif, *J. Fluoresc.*, **2017**, *27*, 31–58.

7 S. H. Park, N. Kwon, J. H. Lee, J. Yoon and I. Shin, *Chem. Soc. Rev.*, **2020**, *49*, 143–179.

8 Y. Wang, L. Zhang, X. Han, L. Zhang, X. Wang and L. Chen, *Chem. Eng. J.*, **2021**, *406*, 127166.

9 S. Oh, J. Jeon, J. Jeong, J. Park, E.-T. Oh, H. J. Park and K.-H. Lee, *Anal. Chem.*, **2020**, *92*, 4917–4925.

10 H. Park, E.-T. Oh, J. Park, S. Subedi, H. J. Park and K.-H. Lee, *Anal. Chem.*, **2025**, *97*, 5982–5991.

11 H. Park, S. Subedi, E.-T. Oh, H. J. Park and K.-H. Lee, *Microchem. J.*, **2024**, *200*, 110375.

12 P. K. Mehta, H. Park, E.-T. Oh, H. J. Park and K.-H. Lee, *Sens. Actuators B*, **2023**, *385*, 133670.

13 S. K. Ko, Y. K. Yang, J. Tae and I. Shin, *J. Am. Chem. Soc.*, **2006**, *128*, 14150–14155.

14 J. Hu, Z. Hu, S. Liu, Q. Zhang, H. W. Gao and K. Uvdal, *Sens. Actuators B*, **2016**, *230*, 639–644.

15 M. Deng, D. Gong, S.-C. Han, X. Zhu, A. Iqbal, W. Liu, W. Qin and H. Guo, *Sens. Actuators B*, **2017**, *243*, 195–202.

16 Z. Zhang, Y. Li, H. Zuo, C. Wang and Y. Shen, *J. Photochem. Photobiol. A*, **2017**, *332*, 293–298.

17 Q. Zou and H. Tian, *Sens. Actuators B*, **2010**, *149*, 20–27.

18 L. Lan, Q. Niu and T. Li, *Anal. Chim. Acta*, **2018**, *1023*, 105–114.

19 S.-L. Pan, K. Li, L.-L. Li, M.-Y. Li, L. Shi, Y.-H. Liu and X.-Q. Yu, *Chem. Commun.*, **2018**, *54*, 4955–4958.

20 Q. Zhang, Y. Li, H. Zuo, C. Wang and Y. Shen, *Analyst*, **2015**, *140*, 2778–2784.

View Article Online
DOI: 10.1039/D6OB00170J

21 C. Kan, X. Shao, F. Song, J. Xu, J. Zhu and L. Du, *Microchem. J.*, **2019**, *150*, 104142.

22 M. Zhao, Y. S. Guo, G. D. Fu, Q. Wang, W. L. Sheng and D. S. Guo, *Microchem. J.*, **2021**, *171*, 106855.

23 Y. K. Yang, S. K. Ko, I. Shin and J. Tae, *Nat. Protoc.*, **2007**, *2*, 1740–1745.

24 M. Tian, C. Wang, Q. Ma, Y. Bai, J. Sun and C. Ding, *ACS Omega*, **2020**, *5*, 18176–18184.

25 M. Matsushita, M. M. Meijler, P. Wirsching, R. A. Lerner and K. D. Janda, *Org. Lett.*, **2005**, *7*, 4943–4946.

26 L. Li, H. Ouyang, Z. Long, Q. Zhang, Y. Jiang, M. Cai, S. Xiong, S. Peng, G. Xu and Q. He, *Org. Biomol. Chem.*, **2023**, *21*, 5560–5566.

27 S. Fang, L. Zhang, Y. Zhao, X. Zhang, L. Zhang, L. Chen, J. Yoon and S. Liu, *Sens. Actuators, B*, **2024**, *411*, 135768.

28 A D. B. Christopher Leslee, U. Venkatachalam, J. Gunasekaran, S. Karuppannan and S. B. Kuppannan, *Org. Biomol. Chem.*, **2023**, *21*, 4130–4143.

29 Z. Ruan, X. Dong, T. Long, S. Liu, Y. Chen and J. Lin, *J. Mater. Chem. C*, **2024**, *12*, 7572–7579.

30 X. Zhang, Y. Zhang, J. Zhao, H. Li and L. Chen, *J. Mater. Chem. C*, **2018**, *6*, 773–780

31 Z. Ruan, C. Fan, X. Wang, D. Shao, X. Yang, W. He, T. Xu, J. Lin and Z. Tian, *Dyes Pigm.*, **2024**, *222*, 111835

32 S. W. Lee, S. Y. Lee and S. H. Lee, *Tetrahedron Lett.*, **2019**, *60*, 151048.

33 S. Subedi, L. N. Neupane, H. Yu and K.-H. Lee, *Sens. Actuators B*, **2021**, *338*, 129814.

34 S. Subedi, L. N. Neupane, P. K. Mehta and K.-H. Lee, *Dyes Pigm.*, **2021**, *191*, 109374.

35 X. Guo, J. Huang, Y. Wei, Q. Zeng and L. Wang, *J. Hazard. Mater.*, **2020**, *381*, 120969.

36 L. N. Neupane, J. Park, P. K. Mehta, E.-T. Oh, H. J. Park and K.-H. Lee, *Chem. Commun.*, **2020**, *56*, 2941–2944.

37 G. L. Long and J. D. Winefordner, *Anal. Chem.*, **1983**, *55*, 712A–724A.

38 H. Park, E.-T. Oh, J. Park, S. Subedi, H. J. Park and K.-H. Lee, *Anal. Chem.*, **2025**, *97*, 5982–5990.

39. S. Uchiyama, T. Santa, T. Fukushima, H. Homma and K. Imai,
J. Chem. Soc., Perkin Trans. 2, **1998**, 2165–2174.

40 P. K. Mehta, K. Ryu, C. K. Kim and K.-H. Lee, *New J. Chem.*, **2022**, *46*, 7003–7013.

41 W. Zhai, X. Sun, T. D. James and J. S. Fossey, *Chem. Asian J.*, **2015**, *10*, 1836–1848.

View Article Online
DOI: 10.1039/D6OB00170J

42 R. C. Larock, *Organomercury Compounds in Organic Synthesis*, Springer-Verlag, Berlin, 1985, pp. 15–16.

43 K. Torssell, *Acta Chem. Scand.*, **1959**, *13*, 115–119.

View Article Online
DOI: 10.1039/D6OB00170J

Data Availability Statement

All experimental and spectroscopic data supporting this study, including NMR spectra, HRMS data and fluorescence measurements, are available in the Supporting Information.